Biosystems Engineering 237 (2024) 157–169

Contents lists available at ScienceDirect

Biosystems Engineering

journal homepage: www.elsevier.com/locate/issn/15375110

Research Paper

Data fusion of FT-NIR spectroscopy and Vis/NIR hyperspectral imaging to predict quality parameters of yellow flesh "Jintao" kiwifruit

Chiara Cevoli [a,b,*], Eleonora Iaccheri [a,b], Angelo Fabbri [a,b], Luigi Ragni [a,b]

[a] Department of Agricultural and Food Sciences, University of Bologna, P.zza Goidanich 60, 47521, Cesena, FC, Italy
[b] Interdepartmental Centre for Agri-Food Industrial Research, Alma Mater Studiorum, University of Bologna, Via Quinto Bucci 336, Cesena, 47521, Italy

ARTICLE INFO

Keywords:
NIR spectroscopy
Hyperspectral imaging
Data fusion
Fruit quality
Yellow kiwifruit
Non-destructive quality assessment

ABSTRACT

The internal quality of kiwifruit, in terms of soluble solid content (SSC), flesh firmness (FF), and dry matter (DM), is widely recognised as a key feature for fruit sorting and pre-harvest assessment. Furthermore, flesh hue (FH) is another important parameter to consider for yellow flesh kiwifruits. NIR and VIS/NIR spectroscopic techniques are valuable alternatives for rapid and non-destructively prediction of all these quality parameters in fruit. Accordingly, the aim of this work was to build a partial least square (PLS) regression models to estimate SSC, FF, FH, and DM of yellow fleshed *Actinida chinensis* (*Jintao*) starting from Vis/NIR hyperspectral imaging (400–1000 nm) and FT-NIR (800–2500 nm) spectroscopy data. To take advantage of the complementary information of the two different spectral ranges, data fusion strategies were investigated to concatenate the data before PLS models. In particular, two different sequential fusion methods were used: low-level data fusion based on the concatenation of the pretreated spectra, and mid-level feature fusion characterised by the concatenation of features (scores) obtained by principal component analysis (PCA) or PLS models developed considering individually each data set. For all quality parameters, the best results were achieved by adopting the second approach of mid-level data fusion (PLS scores), reporting R^2_p (test set validation) of 0.914 (RMSEP=0.97°Brix), 0.843 (RMEP=1.82°H), 0.866 (RMSEP=9.41N), and 0.854 (RMSEP = 0.64%) for SSC, FH, FF, and DM, respectively. Furthermore, with respect to the PLS models from the individual data sets, the results reported a mean RMSEP reduction of 16.0 ± 4.8%, confirming the potential of the data fusion in improving the PLS prediction power for the quality parameter of kiwifruit.

1. Introduction

Actinidia chinensis is a yellow-gold flesh, smooth skinned, and hairless fruit characterised by a sweeter and more aromatic flavour compared to the green flesh and hair skin *Actinidia deliciosa* (Testolin & Ferguson, 2009). For *A. chinensis*, correct harvesting involves a longer post-harvest storage with proper development of ripening stages (McGlone et al., 2007), which is useful to reduce the variability in quality and improve the characteristics of the fruit (Feng et al., 2011). Considering harvest needs, *A. chinensis* is more productive but less vigorous than *A. deliciosa*, with different agricultural demands (Testolin & Ferguson, 2009). The ripening stages of both *A. deliciosa* and *A. chinensis* have some similar aspects concerning changes in quality parameters in terms of dry matter and soluble solid content connected to starch versus sugar conversion also involving softening, but also modifications mainly related to the flesh fruit colour (Feng et al., 2011). Yellow-fleshed *A. chinensis* undergoes a typical colour related modification during ripening, and the variety grows green and turns yellow during veraison. If harvested too early, *A. chinensis* remains green with the consequent loss of its peculiar characteristic strictly linked to consumer acceptance and sensorial traits (Feng et al., 2011). In contrast, if harvested too late it is yellow but softens, resulting in a limited storage time. Therefore, the optimal harvesting time must be based on the compromise between colour change and consistency. This decision differs considerably in the case of *A. deliciosa* for which the flesh colour has no contribution (Testolin & Ferguson, 2009). Accordingly, the internal quality of kiwifruit during ripening is widely recognised as a very important feature for pre-harvest assessment and consequently post-harvest management (Benelli et al., 2022; Feng et al., 2011; McGlone et al., 2007).

Non-destructive techniques can be a valuable alternative for a rapid evaluation of fruit quality and to define the harvesting time, particularly

* Corresponding author. Department of Agricultural and Food Sciences, University of Bologna, P.zza Goidanich 60, 47521, Cesena, FC, Italy.
E-mail address: chiara.cevoli3@unibo.it (C. Cevoli).

https://doi.org/10.1016/j.biosystemseng.2023.12.011
Received 20 July 2023; Received in revised form 19 December 2023; Accepted 23 December 2023
Available online 27 December 2023

if measurements can be carried out directly in the field. Several techniques based on spectroscopic data collection using different instruments exploiting electromagnetism principles have been explored and implemented on *Actinidia* fruits (Berardinelli et al., 2021; O'Toole et al., 2015; Ragni et al., 2010, 2012; Valero et al., 2004). Among these technologies, vibrational spectroscopy in the near infrared (NIR) range is undoubtedly the most widely used technique for internal quality assessment of *Actinidia* (Afonso et al., 2022; Ciccoritti et al., 2019; Feng et al., 2011; Qiang et al., 2010; Schaare & Fraser, 2000; Yang et al., 2019).

Table 1 lists various studies over the last 15 years with Vis/NIR or NIR spectroscopy to evaluate the quality parameters of *Actinidia deliciosa* and *Actinidia chinensis*. Techniques, wavelength ranges, quality parameters, statistical approaches, and the main results allow for easy comparison between studies. From Table 1, it is evident that many authors have investigated yellow fleshed kiwifruits both post-harvest (McGlone et al., 2007; Schaare and Fraser, 2000b; Serranti et al., 2017) and pre-harvest (Afonso et al., 2022; Feng et al., 2011; McGlone et al., 2007; Shafie et al., 2015).

The aforementioned literature demonstrates that both spectral ranges, Vis/NIR (~400–1000 nm) and NIR (~800–2500), can be used to evaluate quality parameters in kiwifruit. Currently, a typical spectroscopy or hyperspectral imaging system rarely covers the visible and near-infrared regions from 400 to 2500 nm due to the challenge of making a sensor that is sensitive to this wide spectral range. However, since a wide spectral range would usually provide more comprehensive and useful information of tested samples, it makes sense to use two detectors that are sensitive to wavelength ranges of 400–1000 nm and 900–2500 nm, respectively. Furthermore, the penetration depth that characterises energy transmission into the fruit can significantly vary with wavelength (Almeida et al., 2006) and with the chemical-physical attributes of the fruit itself. Lammertyn, Peirs, De Baerdemaeker, and Nicolaï (2000) reported that, for apples, Vis/NIR has a stronger penetration depth than NIR. Considering the drawback related to the overlapping signal, Vis/-NIR (up to 1000 nm) is characterised by the presence of weak and highly overlapping signals (3rd overtone) that are not conducive to subsequent feature wavelength selection and model building. Conversely, the NIR range (from 1000 nm) contains the signals corresponding to the 1st and the 2nd overtones, which appear as comparatively less-overlapped and stronger bands, making model optimisation easier (Mishra et al., 2021). In the light of this, the two spectral ranges have their own advantages and disadvantages.

With the help of data fusion approaches, the acquired spectral data with different wavelength ranges can be fused to provide complementary information in order to develop a more accurate and robust predictive model (Li et al., 2023).

Data fusion is an emerging branch of chemometrics that analyses the combination of information provided by different instruments, since various sources of data usually can provide more detailed and potentially complementary information compared with a single technique (Li et al., 2021). Furthermore, data fusion can have many advantages over the processing of individual matrices. For example, the increase in information due to the additional blocks may help reduce the impact of spurious variability sources or potential interferences with a reduction in prediction errors (Biancolillo et al., 2019). Three different strategies can be used to fuse the data, commonly named low-level data fusion, mid-level feature fusion, and high-level decision fusion (Fig. 1). At the low level, data blocks collected from different sensors for the same

Table 1
Some application of Vis/NIR or NIR spectroscopy in assessing the quality parameters of kiwi fruits.

Kiwi variety	Quality parameters	Harvest time	Techniques	Wavelength range (nm)	Statistic approach	Accuracy		References
						R^2	RMSE	
Actinidia Zhonghua	DM	Post-harvest	Spectrometer	1000–2500	PLS	0.90	0.53%	Qiang et al. (2010)
Actinidia Xuxiang	SSC	Post-harvest	Portable spectrometer	350–1100	PLS	0.897	0.90%	Yang et al. (2019)
A. deliciosa, Hayward Bo-Erica®	SSC DM TA	Post-harvest	Spectrometer	850–2500	PLS	0.99 0.98 0.933	0.4 °brix 0.33% 6.65%	Ciccoritti et al. (2019)
Hayward Actinidia	SSC FF	Post-harvest	HSI	400–1000	PLS PLS	0.85–0.94 0.82–0.92	1.10–0.73°brix 14.51–9.87 N	Benelli et al. (2022)
Xuxiang, Hongyang Cuixiang green Actinidia	FF SSC pH	Post-harvest	HSI	380-1023 874-1734	PLS, MLR, SVM	0.98 (MLR) 0.95 (MLR) 0.9 (SVM)	36.32 N cm^{-2} 0.4°brix 0.01	Zhu et al. (2017)
Actinidia deliciosa Actinidia chinensis	DM	In orchard	Portable spectrometer	300–1150	PLS	0.88	1.22%	Shafie et al. (2015)
Actinidia, cultivar G3	Fruit ripening	Post-harvest	HSI	900–1700	PCA			Serranti et al. (2017)
Actinidia chinensis 'Hort16A' yellow fleshed	DM SSC FH	Pre-harvest (PH) Harvest (H)	Spectrometer	300–1140	PLS	0.91 (PH), 0.97 (H) 0.92 (PH), 0.93 (H) 0.88 (PH), 0.88 (H)	0.4% (PH), 0.24% (H) 0.71% (PH), 0.31% (H) 1.05°H (PH), 0.98°H (H)	McGlone et al. (2007)
Actinidia chinensis	SSC Density FH	Post-harvest	Spectrometer	300–1100	PLS	0.93 0.74 0.82	0.8 °brix 3.6 kg m-3 1.6°H	Schaare and Fraser (2000)
Actinidia chinensis 'Hort16A'	DM SSC FH	In orchard	Portable spectrometer	588–1092	MLR	0.85 0.90 0.86	0.60% 0.90% 1.4°H	Feng et al. (2011)
Actinidia chinensis Planch Jintao	DM SSC FF TA Flesh colour (a*) pH	In orchard	Spectrometer	345–1037	PLS	0.65 0.81 0.57 0.12 0.85 0.45	1.19% 1.27 °brix 9.47 N 0.19% 1.35 0.12	Afonso et al. (2022)

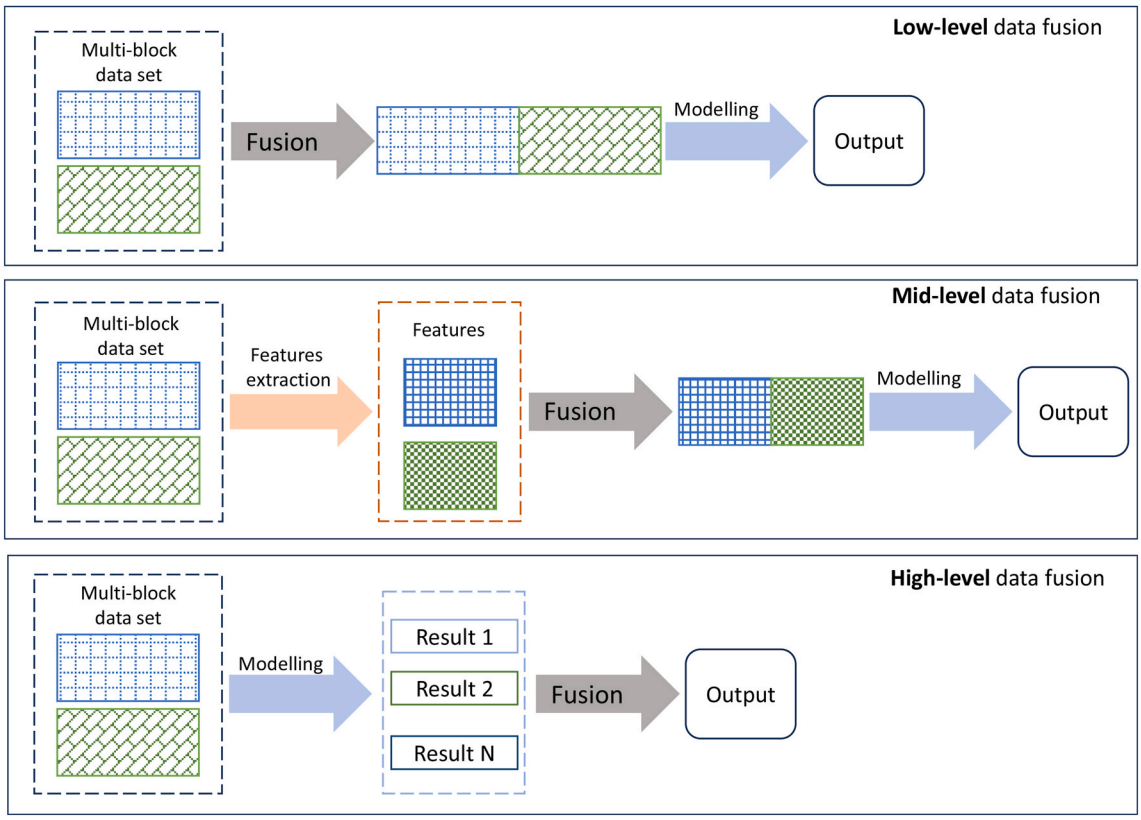

Fig. 1. General scheme describing low, mid and high-level data fusion.

samples are directly concatenated into a single matrix (after proper pre-processing) to obtain a new, larger data set. In the mid-level, the data fusion is performed after compression or reduction of the data (feature selection) of each block to be fused. The feature selection introduces an additional step in the modelling due to the choice of the feature extraction procedure that is able to limit loss of information. In high level fusion, models are separately developed for each data block and the respective results are integrated into a single final response. This last data fusion level is mainly used for classification problems (Brown, 2020).

Starting from these considerations, the main aim of this study was to explore the application of two sets of spectral range data (Vis/NIR and FT-NIR) in combination with data fusion strategies to predict the quality parameters (flesh firmness (FF), soluble solid content (SSC), flesh hue (FH) and dry matter (DM)) of yellow fleshed *Actinida chinensis, Jintao*.

First, data from individual instrumental techniques (Vis/NIR hyperspectral camera and FT-NIR spectrometer) were separately considered; next, to take advantage of the complementary information connected to different spectral ranges, low and mid-level fusion strategies were implemented to concatenate the data into a single regression model.

From point of view of industrial applications, the combination of a Vis/NIR hyperspectral camera and FT-NIR spectrometer would allow to evaluate internal, dimensional, and surface quality indices (e.g. colour or any defects identifiable with RGB images) at the same time. Hyperspectral cameras in the Vis/NIR range also allow to acquire RBG images with acceptable resolution. The reason in using the HSI in the VIS/NIR and not in the full NIR range is mainly due to an economic issue, given that the cost of a NIR-HSI camera (1000–2500 nm) is around 5 times higher than that of a Vis/NIR-HSI camera.

2. Materials and methods

2.1. Samples

230 Yellow-fleshed kiwifruits (*Actinidia chinensis* Planch '*Jintao*') were collected from more than 8 orchards located in different Italian regions during the commercial harvest season (8 samplings from October to December 2022). Multiple orchards allowed us to simultaneously include several sources of variability (soil, weather conditions, cultural practices) in our study. The company did not provide any specific information about the geographical location of the orchards.

All kiwi samples were analysed within two days after harvest. The fruits were weighed (96.37 ± 17.95 g) and dimensionally characterised measuring the longitudinal (71.1 ± 5.8 mm) and mean equatorial diameter (47.7 ± 3.2 mm). Subsequently, non-destructive acquisitions (FT-NIR spectroscopy and Vis/NIR HSI) and destructive quality measurements (Magness-Taylor force, soluble solid content, flesh hue, and dry matter) were performed on the same side of each fruit (environmental temperature of 20 ± 2 °C).

2.2. Vis/NIR hyperspectral imaging

A push-broom linear array hyperspectral camera (Nano-Hyperspec VNIR, Headwall Photonics, Inc., Fitchburg, MA, USA) was used to acquire hyperspectral images. The camera operates in the wavelength

range of 400–1000 nm and is characterised by 272 bands and a spatial resolution of 640 points. A focal lens of 17 mm was mounted on the camera, which was installed at a height of 54 cm from the underlying conveyor belt, running at 8 mm s^{-1}. The light source consisted of two halogen lamps (120 W) that were installed at a distance of about 30 cm from the conveyor belt plane. Exposure time and frame period were set at 30 ms according to the light intensity. The reflectance of white (*Rw*) and dark (*Rd*) reference materials was used to calibrate the camera. The calibrated diffuse reflectance spectrum (R_C), was calculated from the raw diffuse reflectance spectrum (R_R) of each sample using the following equation:

$$R_C = \frac{R_R - R_D}{R_W - R_D} \quad (1)$$

For each image, the region of interest (ROI) was selected using k-means clustering, performed by adopting 3 clusters (classification method: Euclidean distance): i) background, ii) shaded edge of the kiwi, and iii) ROI. Finally, the mean spectra were calculated considering the ROI spectra and used for subsequent elaboration.

2.3. FT-NIR spectroscopy

Diffuse reflectance spectra in the range from 833 to 2500 nm (0.27 nm resolution) were acquired as an average of 32 scans using a FT-NIR spectrophotometer (MA- TRIX ™ – F, Bruker Optics). Two scans were obtained by placing the optical fibre probe (IN 261, Bruker Optics, Mass., USA) in direct contact with the kiwi surface at two different points of the same fruit side. The background spectrum, corresponding to the spectralon material, was subtracted from each spectrum. The mean spectrum of the two acquisitions was calculated and used for the elaboration.

2.4. Destructive measurements of reference parameters

After Ft-NIR spectroscopy and Vis/NIR HSI acquisitions, kiwi quality parameters were measured by destructive methods. Specifically, FF, SSC, FH, and DM were considered. FF was measured using a compression test (on the same side as the spectroscopy and HSI) performed with a texture analyser (TA-HDi, Stable Micro System Ltd., Godalming, UK) equipped with a cylindrical steel probe (8 mm) with a hemispherical head (ASABE Standard, 2018). According to the procedure adopted by the company, the test was performed at a speed of 10 mm s^{-1} and up to a deformation of 8.9 mm. Before the analysis, 1 mm of skin was removed in the test area.

Subsequently, on the same kiwi and side, the SSC (°Brix) of the juice was measured by a digital refractometer (PR-101 Digital Refractometer, ATAGO CO., LTD, Tokyo, Japan), while the FH was calculated from the x, y, z colour coordinates measured using a Minolta Chroma Meter (CR-400, D65 light source) after the removal of 2 mm of skin.

Finally, DM was measured using a slice of about 1.5 mm in thickness radially cut along the fruit equator. The slice was weighed immediately after cutting and then after dried in oven at 65 °C to constant weight (generally 24 h).

Correlations between quality indexes (FF, SSC, FH, and DM) were investigated using a Pearson correlation matrix.

2.5. Chemometric models

Considering the mean Vis/NIR spectra, the range from 400 to 450 nm was removed due to a low signal-to-noise ratio produced by the sensor. Subsequently, reflectance data were smoothed (Savitzky-Golay method; polynomial order: 2; smoothing points: 7) to reduce noise from the spectra (S), normalised by standard normal variate (SNV) method (reduction of the spectral variability between samples due to differences in optical path and scattering), and pre-processed by applying the Savitzky–Golay derivative (first=D1 or second=D2) to remove both additive and multiplicative effects. Finally, the spectral data were mean centred (MC).

For the FT-NIR spectra, the last part of the spectra from 2200 to 2500 nm was deleted as it was characterised by higher instrumental noise. Furthermore, the spectra were smoothed (S) and pre-processed by D1 or D2 and MC. Subsequently, PLS regression models were developed to estimate the quality indexes (FF, SSC, FH, and DM), starting from individual Vis/NIR or FT-NIR data matrices.

Furthermore, considering that two blocks of data (Vis/NIR and FT-NIR) were collected on the same sample set, the possibility of integrating the information present in the different matrices (data fusion) into a single model may improve the prediction power. Two different data fusion approaches were implemented. In the first (low-level data fusion), the Vis/NIR and FT-NIR data sets, after proper pre-treatment, were combined to build a unique matrix that was then scaled (weighting and mean centring) and finally subjected to PLS regression. The main drawback of low-level fusion is the high variable number of the final matrix that may not compensate for irrelevant or spurious variance brought by the addition of the same blocks. A careful variable selection might remove redundant or unnecessary data and improve estimation accuracy by effectively identifying the subset of important predictors and enhancing the model's interpretability with parsimonious representation. Variable importance on projection (VIP) scores estimates the importance of each variable in the projection used in a PLS model, and variables with VIP scores greater than 1 are commonly considered important in the prediction. This criterion is often used for variable selection. Accordingly, variables characterised by VIP scores higher than 1 were selected and new PLS models were developed.

In the second data fusion method (mid-level feature fusion), concatenation of the two data sets was performed after compression of the data contained in each block. Data compression (feature selection) was performed by two approaches:

1) Principal component analysis (PCA) was performed after proper pre-treatment. Scores corresponding to the PCs covering the 99% of the variance were extracted as features through 10-fold cross-validation for individual Vis/NIR and FT-NIR data and then concatenated to build a unique matrix that was scaled (weighting and mean centring) and subjected to PLS regression;
2) For each quality index, PLS regressions for individual Vis/NIR and FT-NIR data were performed after proper pre-treatment. Scores corresponding to the selected number of latent variables (LVs) were extracted as features through 10-fold cross-validation and then concatenated to build a unique matrix which was scaled (weighted and mean centred) and finally subjected to PLS regression, obtaining global matrices characterised by 21 (SSC), 16 (FH), 19 (FF), and 22 (DM) x-variables.

The flowchart of the stages adopted to develop all the PLS models starting from individual data sets or concatenated blocks after fusion procedures is shown in Fig. 2. For all the PLS models, the original data set (n=230) was split into a calibration/cross validation (venetian blind cross-validation method, segments: 10) set (75% of the sample, n=172) and a test set validation (25% of the samples, n=58), using the Kennard-Stone method (selects samples that best span the same range as the original data, but with an even distribution of samples across the same range) (Daszykowski et al., 2002).

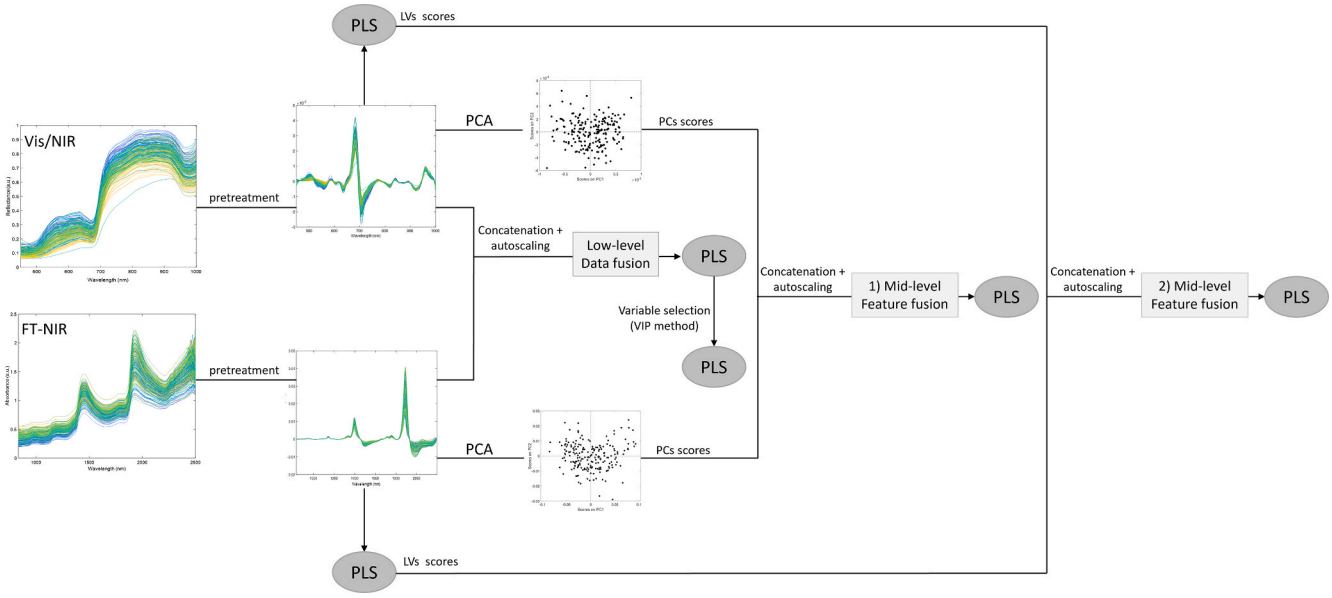

Fig. 2. Flowchart of the different steps of the data fusion adopted in the study.

The optimal number of LV was identified according to the minimum of the RMSECV curves. Furthermore, the significance of the PLS models, as a function of the number of LV, was evaluated by permutation test (Pairwise signed rank test), thus providing the probability that the original model (unpermuted) is significantly different from the one built under the same conditions but using random data (permuted model). This procedure allows to identify overfitting.

PLS results were analysed in terms of determination coefficient (R^2), root mean square error (RMSE), and residual prediction deviation (RPD):

$$R^2 = \frac{\sum_{i=1}^{N}(\hat{y}_i - \bar{y})^2}{\sum_{i=1}^{N}(y_i - \bar{y})^2} \quad (2)$$

$$RMSE = \sqrt{\frac{\sum_{i=1}^{N}(\hat{y}_i - \bar{y})^2}{N}} \quad (3)$$

$$RPD = \frac{SD}{RMSE} \quad (4)$$

where y_i is the actual quality parameter, $\hat{y}_i$ is the predicted quality parameter, $\bar{y}$ is the mean of the actual values, N is the number of samples, and SD is the standard deviation of actual quality parameter values.

All the models were developed by using PLS Toolbox for Matlab2018a.

3. Results

Mean, standard deviation (SD), and minimum and maximum values of destructive quality parameters are shown in Table 2. The possible linear correlations between quality parameters were evaluated using

Table 2
Mean, minimum, maximum and standard deviation (SD) of the quality parameters.

	SSC (°Brix)	FH (°H)	FF (kg)	SS (%)
Average	12.88	103.18	3.68	17.71
Standard deviation	3.51	4.51	2.47	1.71
Minimum	4.00	94.96	0.12	13.62
Maximum	19.70	115.60	10.87	21.77

SSC: soluble solid content; FH: flesh hue; FF: flesh firmness; DM: dry matter.

Table 3
Pearson correlation matrix of the quality parameters.

	SSC (°Brix)	FH (°H)	FF (N)	DM (%)
SSC (°Brix)	1			
FH (°H)	−0.855	1		
FF (N)	−0.825	0.665	1	
DM (%)	0.510	−0.582	−0.262	1

SSC: soluble solid content; FH: flesh hue; FF: flesh firmness; DM: dry matter.

Pearson correlation coefficients (Table 3). All correlations were significant at $p < 0.01$, and a higher correlation was achieved between SSC and FH (r=−0.855) and SSC and FF (r=−0.825). Furthermore, less strong correlation was observed between FH and FF (r=0.665).

Concerning the Vis/NIR HSI, the mean reflectance spectra of all samples are shown in Fig. 3 where raw and pre-processed spectra (SNV, D1 and D2) are reported. The visible portion of the spectra (from 400 to 700 nm) is characterised by absorption bands of anthocyanins (450–550 nm) and chlorophyll-α (680 nm) and chlorophyll-β (640 nm) connected to colour samples, and usually adopted as quality attributes to assess fruit ripeness (ElMasry et al., 2007). The NIR section (from 700 to 1000 nm) is characterised by the second and third overtones of fundamental vibration of –OH and –CH. In particular, absorption bands related to water can be identified at 750 (OH third overtone) and 960 nm (OH second overtone), while the small absorption at 840 nm (slight inflection in reflectance spectra) is ascribable to sugar.

Regarding the FT-NIR, Fig. 4 shows the raw and pre-processed (SNV, D1 and D2) absorbance spectra of all samples. The spectra are characterised by overtones and combinations of fundamental vibration of –OH, –CH, and –NH groups. Specifically, five peaks around 974 (OH first overtone), 1200 (CH first overtone), 1460 (OH second overtone), 1780 (CH second overtone) and 1930 nm were identified, according to (Ciccoritti et al., 2019). These peaks are related to the absorption of water, cellulose, and sugars (McGlone & Kawano, 1998). In addition, in this case, the spectral shape was the same for all samples. As for the Vis/NIR, the raw spectra were pre-processed (SNV, D1 e D2) to emphasise the peaks and to remove offset baseline and resolve overlapped peaks.

PLS regression models were developed to estimate the quality indexes (FF, SSC, FH, and DM), starting from Vis/NIR or FT-NIR data by using individual data sets or data fusion approaches (data or feature level). Results of PLS models developed considering the individual data

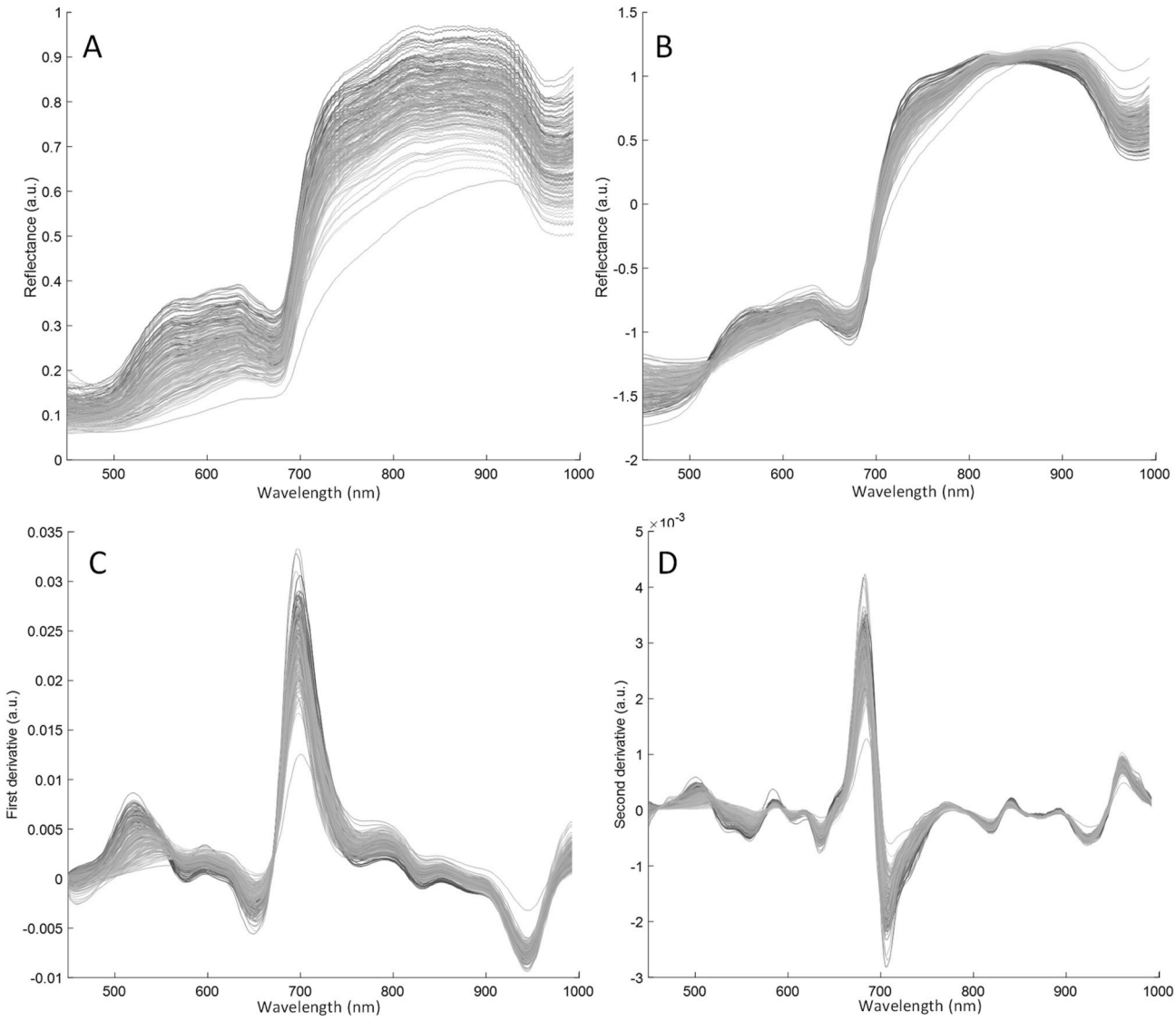

Fig. 3. Mean Vis/NIR HIS spectra: A) raw reflectance, B) Standard Normal Variate (SNV) pretreatment; C) first derivative (D1) pretreatment; D) second derivative (D2) pretreatment.

set are shown in Table 4, according to the pre-treatment type and number of latent variables (LV).

For the Vis/NIR data set, the best results were obtained with the S + D2+MC pre-treatment (R^2_P from 0.704 to 0.859), although, overall, the differences between the two pre-treatments were negligible. Comparable results were achieved starting from absorbance Vis/NIR data (Supplementary material, Table S1).

The FT-NIR data set had the best results adopting a S + D1+MC pre-treatment sequence (R^2_P from 0.731 to 0.889) regardless of the quality parameter. For both data sets, SSC was the parameter with the highest R^2_P (Vis/NIR: 0.859, FT-NIR: 0.889) and RPD (Vis/NIR: 2.7, FT-NIR: 3.7) values.

To identify which spectral portions were most effective in the regression, VIP scores were evaluated. These values quantify the extent of contribution for each variable, and variables with VIP scores greater than 1 are usually considered important in the prediction. VIP scores of all prediction models are shown in Fig. 5 (Vis/NIR) and 6 (FT-NIR). As expected, considering the Vis/NIR range the FH prediction is mainly affected by the visible part up to 750 nm (VIP>1), while for the other parameters, VIP scores higher than one were also observed in the NIR range. Similar VIP score trends were reported by Afonso et al. (2022) for the prediction of the same quality parameters.

Considering the FT-NIR range, spectral ranges characterised by VIP >1 are quite similar, regardless of the quality parameter prediction model. Overall (the raw spectra were pre-treated by S + D1+MC), these ranges are attributable to first and second overtone of –CH and –OH (previously described). New PLS models were developed considering only variables with VIP >1. For both the spectral ranges, the results with and without VIP selection were fully comparable, and only in some cases were the results obtained after VIP selection slightly lower.

Results of PLS models developed by adopting data fusion approaches (low and mid-level) are shown in Table 5. After low level data fusion, the global matrix was composed of 2187 variables. PLS results were better than those obtained by using the individual data sets for all quality parameter (R^2_P from 0.806 to 0.896, RPD from 2.4 to 3.5), except for DM ($R^2_p = 0.672$, RPD=1.7). The VIP method (VIP >1) was used to reduce the data set and to remove redundant and unnecessary information. In particular, the reduction was from 47 (SCC: 1162 variables) to 75% (FH: 546 variables). Spectral ranges characterised by VIP higher than 1 (selected variables) are indicatively the same as shown in Figs. 5 and 6. The application of variable selection to low data level fusion models further improved the results (R^2_P up to 0.905; RPD up to 3.6), reporting a

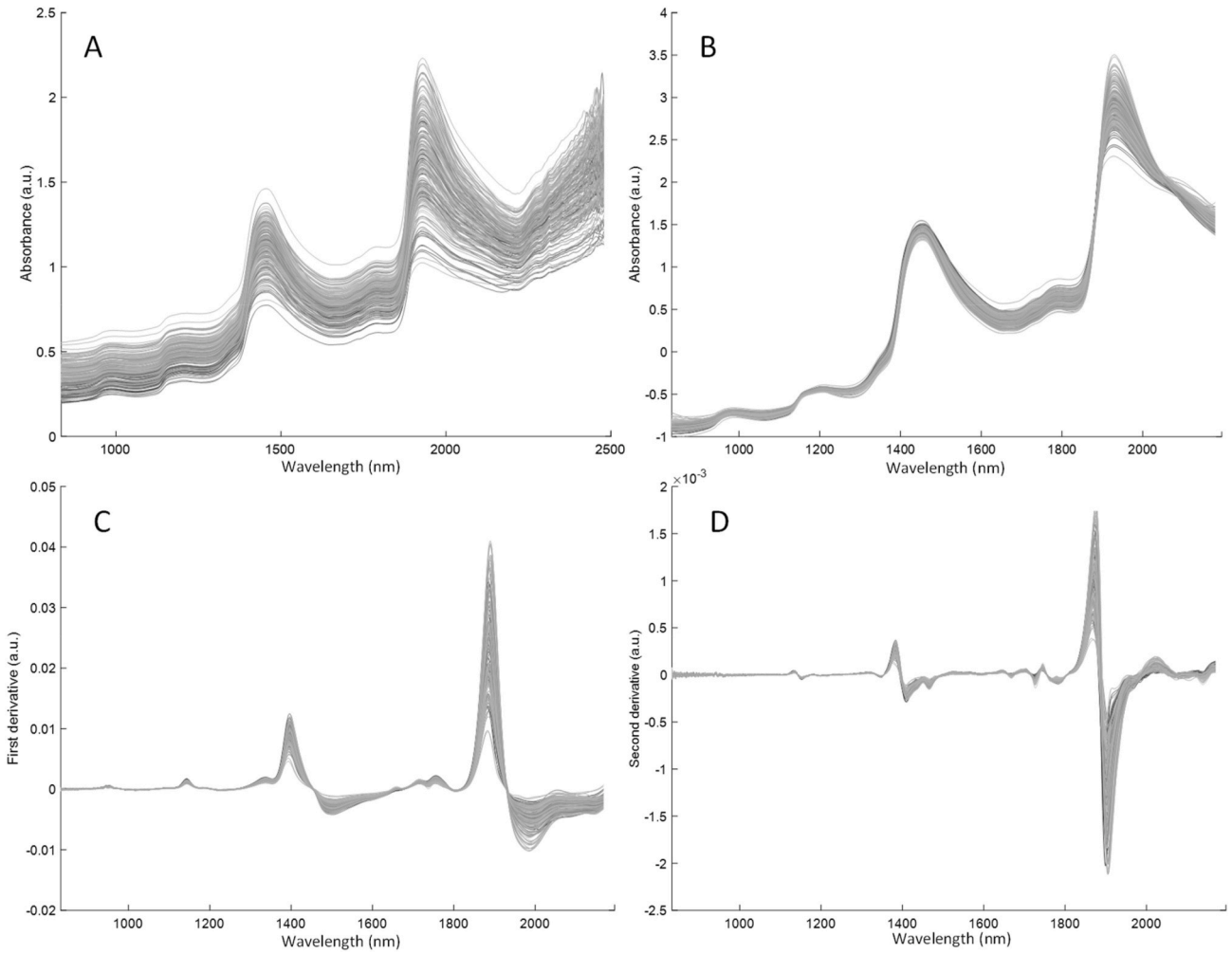

Fig. 4. FT-NIR spectra: A) raw absorbance, B) Standard Normal Variate (SNV) pretreatment; C) first derivative (D1) pretreatment; D) second derivative (D2) pretreatment.

Table 4
Results of the PLS models developed to predict quality parameters, starting from individual FT-NIR or Vis/NIR HSI data matrices.

Technique	Quality parameter	Pretreatment	R_C^2	R_{CV}^2	R_P^2 (n=57)	RMSEC	RMSECV	RMSEP (n=57)	RPD	LVs
Vis/NIR	SSC (°Brix)	S + D1+MC	0.897	0.859	0.842	1.13	1.33	1.42	2.6	13
		S + D2+MC	0.899	0.869	0.859	1.13	1.28	1.34	2.7	11
	FH (°H)	S + D1+MC	0.850	0.806	0.808	1.77	2.02	2.10	2.4	16
		S + D2+MC	0.868	0.824	0.809	1.66	1.93	2.05	2.4	9
	FF (N)	S + D1+MC	0.820	0.789	0.787	10.98	11.86	11.86	2.2	10
		S + D2+MC	0.861	0.814	0.789	9.60	11.17	11.96	2.2	10
	DM (%)	S + D1+MC	0.829	0.783	0.686	0.69	0.78	0.96	1.8	9
		S + D2+MC	0.835	0.782	0.704	0.69	0.79	0.89	1.8	12
FT-NIR	SSC (°Brix)	S + D1+MC	0.934	0.898	0.889	0.92	1.14	1.16	3.4	9
		S + D2+MC	0.867	0.789	0.788	1.32	1.58	1.59	2.2	6
	FH (°H)	S + D1+MC	0.819	0.751	0.731	1.96	2.31	2.31	1.9	8
		S + D2+MC	0.791	0.668	0.632	2.10	2.67	3.01	1.6	6
	FF (N)	S + D1+MC	0.857	0.802	0.804	9.70	11.37	10.78	2.4	8
		S + D2+MC	0.878	0.759	0.691	8.93	12.64	13.13	1.8	8
	DM (%)	S + D1+MC	0.838	0.767	0.747	0.69	0.83	0.84	2.0	9
		S + D2+MC	0.815	0.681	0.610	0.74	0.94	1.11	1.6	5

SSC: soluble solid content; FH: flesh hue; FF: flesh firmness; DM: dry matter; R^2: determination coefficient; RMSE: root mean square error; RPD: residual prediction deviation; latent variables LVs; *C*:calibration; *CV*: cross-validation; *P*: external validation.

mean RMSEP reduction of 15.0 ± 1.3% than the models developed with the individual data sets. As for the individual data set models, the best results were achieved for SSC, and the worse was achieved for DM.

The mid-level feature fusion was performed by using two different approaches. In the first case, the scores of the first 10 PCs were fused in a single matrix for a total of 20 variables. The cumulative variance captured by the first 10 PCs is shown in Fig. 7 for Vis/NIR and FT-NIR data. In both cases, the 10 PCs describe 99% of variance.

In the second cases, starting from the PLS models developed for each quality index, the scores of the selected LVs were concatenated,

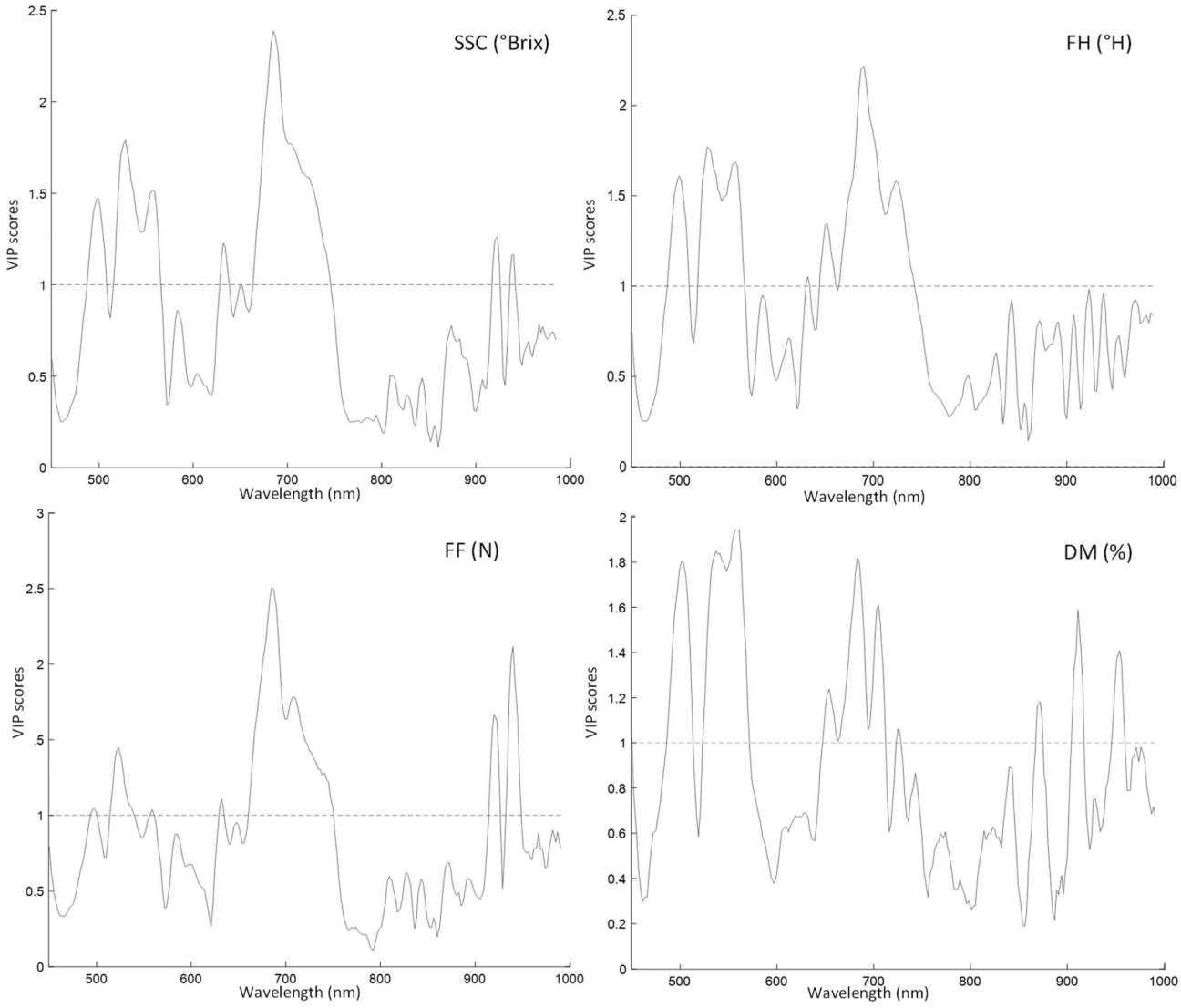

Fig. 5. VIP scores obtained by PLS regression models developed to predict soluble solid content (SSC), flesh hue (FH), flesh firmness (FF) and dry matter (DM) starting from individual Vis/NIR data set (pretreatment: smoothing 7 points, second derivative D2; mean cantering MC).

Table 5
Results of the PLS models developed to predict kiwi quality parameters, starting from the data fusion by low and mid-level approaches.

Fusion level	Quality parameter	Variable number	R^2_C	R^2_{CV}	R^2_P (n=57)	RMSEC	RMSECV	RMSEP (n=57)	RPD	LVs
Low-level	SSC (°Brix)	2187	0.961	0.883	0.896	0.74	1.10	1.05	3.5	8
	FH (°H)	2187	0.896	0.80	0.806	1.53	2.01	1.96	2.4	6
	FF (N)	2187	0.924	0.823	0.848	7.25	10.78	9.51	2.6	8
	DM (%)	2187	0.841	0.691	0.672	0.69	0.97	1.01	1.7	6
Low-level (VIP selection)	SSC (°Brix)	1162	0.961	0.903	0.905	0.74	1.03	0.99	3.6	8
	FH (°H)	546	0.892	0.842	0.832	1.56	1.84	1.85	2.6	5
	FF (N)	547	0.923	0.837	0.829	7.25	10.58	10.88	2.5	7
	DM (%)	617	0.862	0.761	0.704	0.65	0.85	0.89	2.0	5
1) Mid-level (PCA-PCs scores)	SSC (°Brix)	20	0.871	0.866	0.865	1.21	1.34	1.34	2.7	5
	FH (°H)	20	0.777	0.763	0.786	2.11	2.34	2.31	2.2	3
	FF (kg)	20	0.831	0.813	0.823	10.29	10.78	10.58	2.5	6
	DM (%)	20	0.792	0.651	0.631	0.92	1.04	1.08	1.6	5
2) Mid-level (PLS-LVs scores)	SSC (°Brix)	21	0.936	0.913	0.914	0.91	1.07	0.97	3.7	2
	FH (°H)	16	0.863	0.838	0.843	1.73	1.94	1.82	2.7	2
	FF (N)	19	0.870	0.856	0.866	9.51	9.90	9.41	2.9	2
	DM (%)	22	0.866	0.862	0.854	0.63	0.63	0.64	2.7	4

SSC: soluble solid content; FH: flesh hue; FF: flesh firmness; DM: dry matter; R^2: determination coefficient; RMSE: root mean square error; RPD: residual prediction deviation; latent variables LVs; *C*:calibration; *CV*: cross-validation; *P*: external validation.

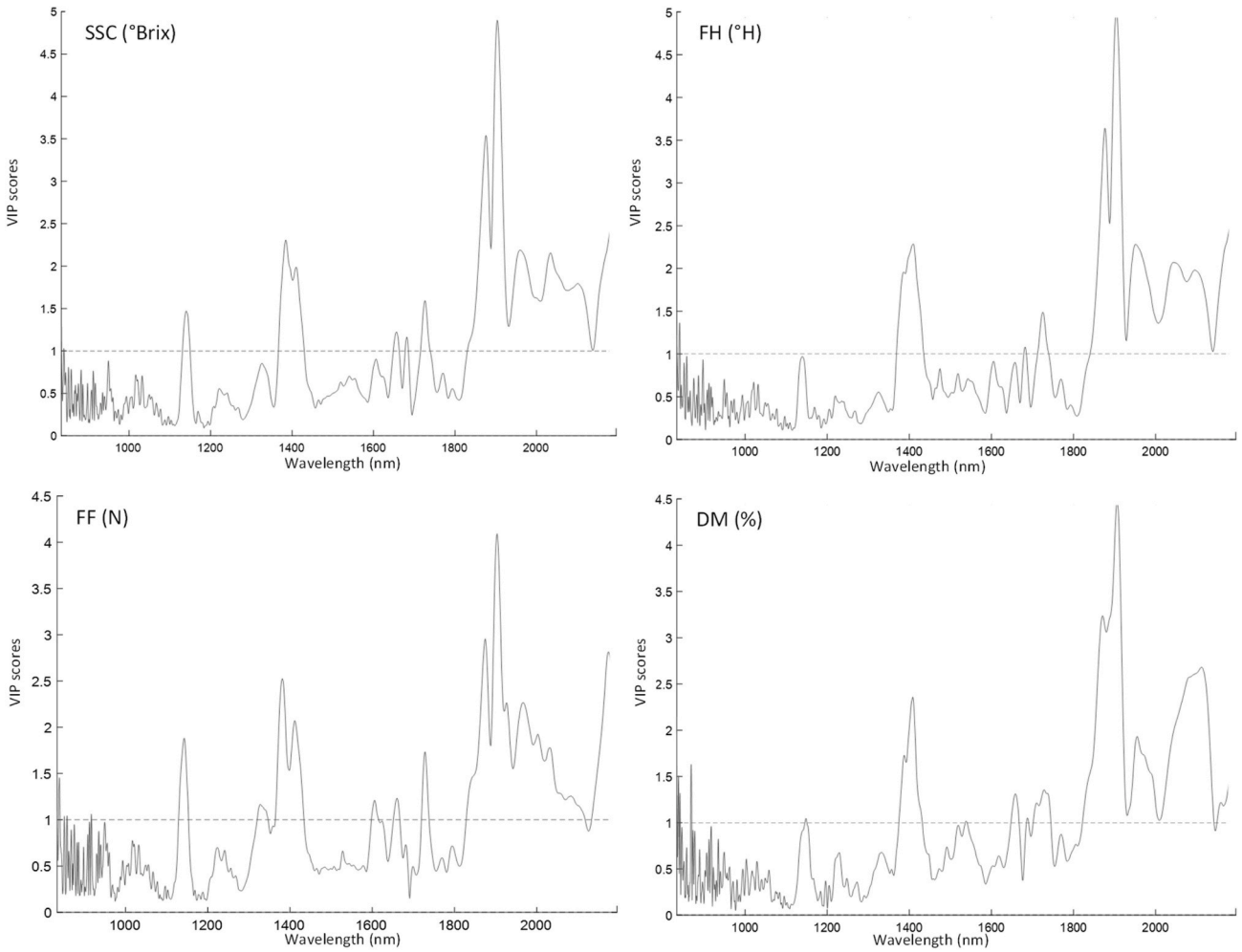

Fig. 6. VIP scores obtained by PLS regression models developed to predict SSC, FH, FF and DM starting from individual FT-NIR data set (pretreatment: smoothing 7 points, first derivative D1; mean cantering MC).

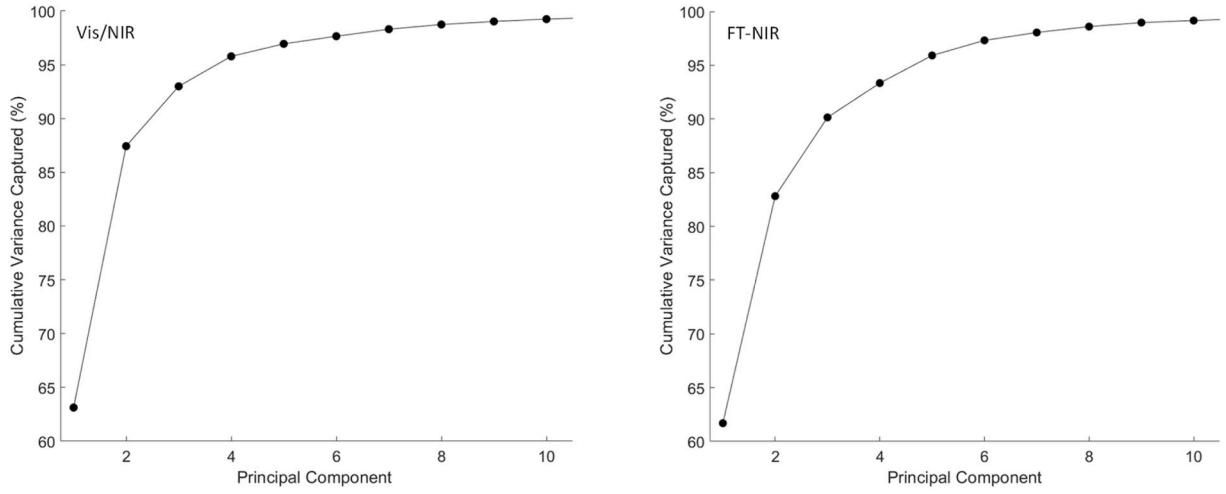

Fig. 7. Cumulative variance (%) captured by the first 10 principal component (PC) obtained by PCA of the individual Vis/NIR and FT-NIR data sets.

obtaining global matrices characterised by 21 (SSC), 16 (FH), 19 (FF), and 22 (DM) x-variables. Adopting the first approach, R_P^2 values equal to 0.914 (RMSEP = 0.07 °Brix), 0.843 (RMSEP = 1.82 °H), 0.866 (RMSEP=9.41 N), and 0.854 (RMSEP=0.64 %) were reached for SSC, FH, FF and DM, respectively. The second approach of mid-level data fusion further improved, with respect to PLS from individual data set, reporting RMSEP reduction up to 13% and 24% for FF and DM, respectively. The R_P^2 of the PLS model developed to estimate DM increased more than 14%, passing from 0.747 to 0.854, confirming the potential of the data fusion in improving PLS prediction power.

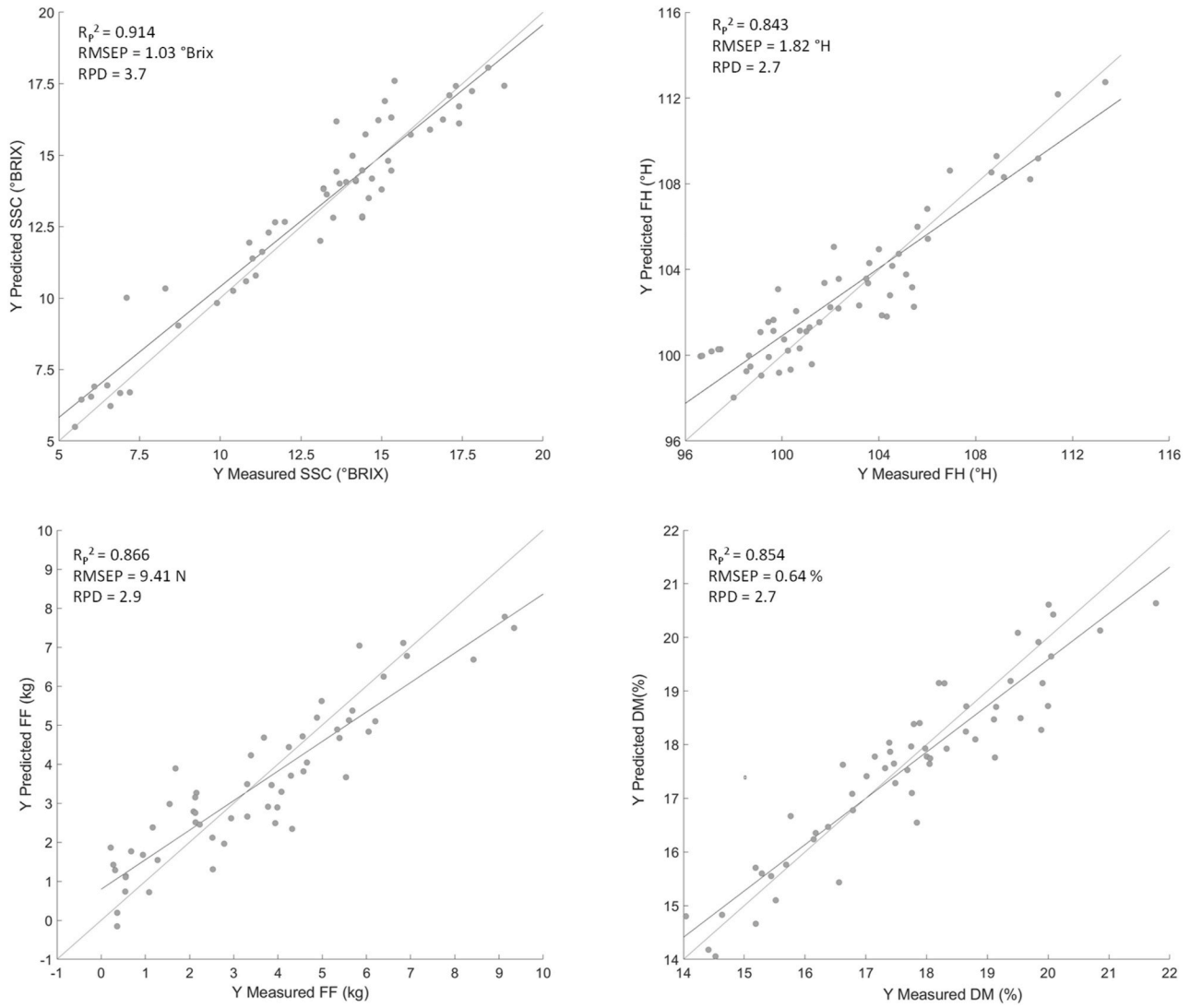

Fig. 8. Measured versus predicted values in external validation (soluble solid content (SSC), flesh hue (FH), flesh firmness (FF) and dry matter (DM)) obtained by PLS models developed after mid-level feature fusion (PLS scores).

Fig. 8 shows the measured *vs.* predicted values (prediction data set) of all quality indices obtained by the best PLS regression. The significance of all PLS models, as a function of the number of LV, was evaluated by permutation test reporting significance values less than 0.01. All the models developed were significant with at least a 99% confidence level. Correlation coefficients between the unpermuted and permuted regression vectors versus the standardised sums-of-squares (SSQ) are shown in Fig. 9 for SSC models (similar results were observed for all the quality indices). In a robust model, cross-validated and self-prediction (calibration) values should be quite close to each other but should be lower than the values calculated for the unpermuted y-block (right side of the plot), independently of the correlation with the reference values. The distance between the unpermuted results and the mean (y-value) is a measure of the robustness of the model. A higher distance indicates a more robust model, which is likely to be overfit. For the mid-level feature fusion, the distance is about 8, while for the other models, it varies from 1 to 5. This confirms that the mid-level fusion approaches produce a more robust model. The worst results, in terms of significance and robustness, were observed for the low-level data fusion.

4. Discussion

The mean values of the quality parameters obtained agree with those reported by (Feng et al., 2011) for yellow-fleshed kiwifruit evaluated pre- and post-harvest. Furthermore, the correlations observed between FH, SSC, and FF confirm that by decreasing the °H value (flesh the colour turns towards yellow), the °Brix increases and the fruit becomes softer.

Results of the PLS models developed considering the individual data sets confirm that both spectral ranges are useful to predict all quality parameters, especially SSC. Comparing the two spectral ranges, the best results were obtained for the FT-NIR data set, except for prediction of yellow flesh colour (FH). In this latter case, PLS results of Vis/NIR spectra were clearly better. FH is a parameter that is directly connected with flesh colour variation, and consequently, as could be expected, the main contribution in the prediction is due to the visible range acquired only by the HSI camera. This is confirmed by the evaluation of VIP scores. FH prediction is mainly affected by the visible portion up to 750 nm (VIP >1), while for all the other parameters VIP scores higher than unity were also observed in the NIR range. Similar VIP score trends were also reported by Afonso et al. (2022) for prediction of the same quality parameters.

Concerning low-level data fusions, it is distinguishing the DM prediction that was not improved by this fusion strategy. It is difficult to identify a motivation for this, especially considering that the literature data report a wide variability in the yellow kiwi DM prediction (R_P^2 from 0.65 to 0.91). Further studies on a larger number of samples, from

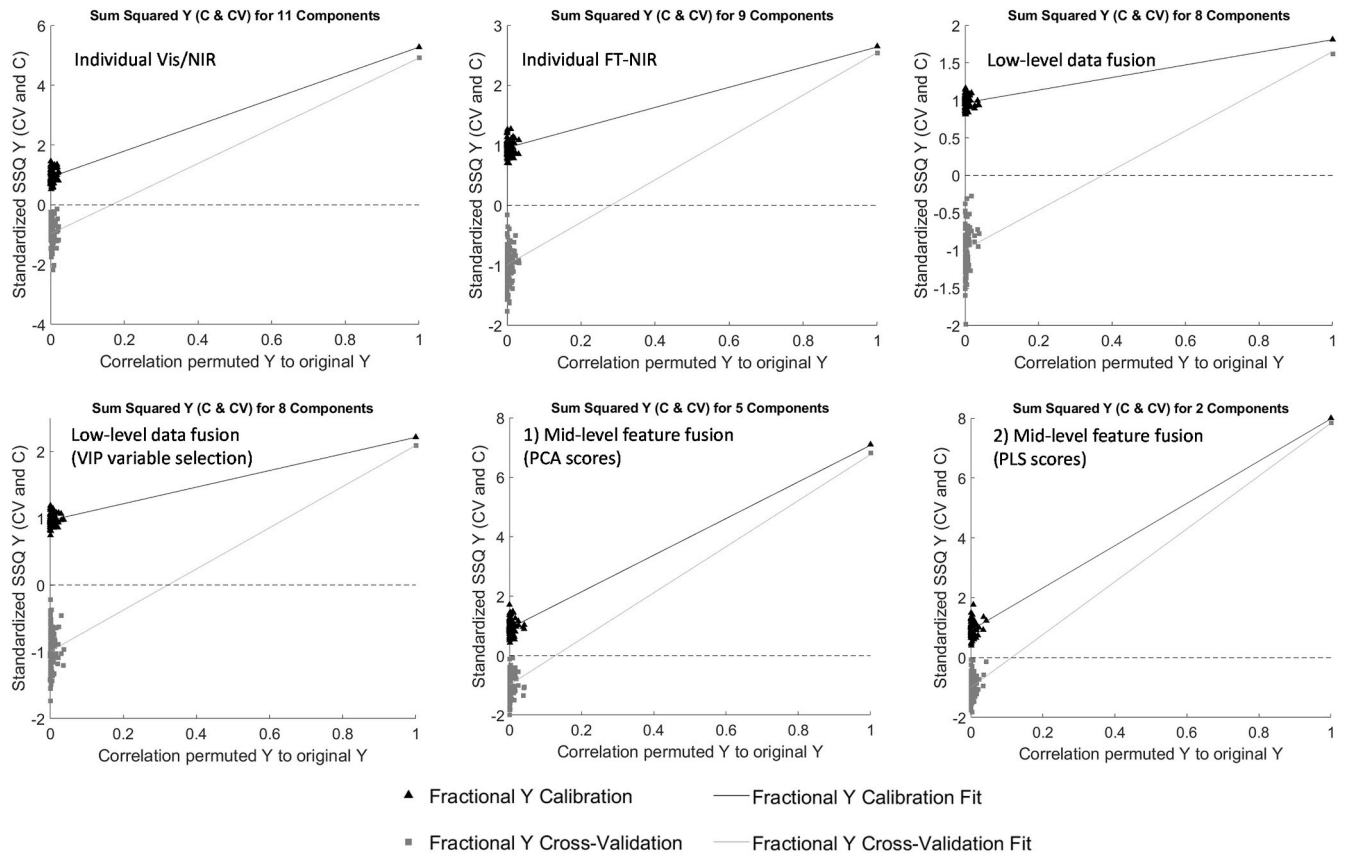

Fig. 9. Permutation test (100 permutations) results of PLS models developed to predict soluble solid content (SCC), considering individually FT-NIR and Vis/NIR data, and after low and mid level fusion (PCA and PLS scores).

several production seasons, could help to understand and, eventually, confirm these results.

Regarding the results obtained after the mid-level feature, the first approach (PCA-PCs scores) gave worse results for all quality indexes than those achieved by all other fusion level models. Probably the PCA decomposition leads to information loss, resulting in poor predictive performance of the fused models. In contrast, the mid-level based on the concatenation of the scores obtained by independent PLS regressions showed the best results for all quality indices. The difficulty with feature level fusion concerns the selection of the optimal feature selection method, and improper methods could lead to information loss, as was observed for the first mid-level approach (PCA-PCs scores). To confirm this, permutation tests showed a higher robustness of the models developed by applying the mid-level fusion approaches compared to those obtained by individual data set or low-level data fusion. Furthermore, lower significance values were observed for the low-level data fusion. This is likely due to the high redundancy and unnecessary information associated with the concatenation of the two individual data sets.

Although there is no statistical basis as to how the threshold equal to two was determined, usually models characterised by RPD values higher than two are considered as excellent. Furthermore, for quality control purposes, the following RPD categories have been identified: i) 2.4–3.0 rough screening quality; ii) 3.1–4.9 screening quality; iii) 5.0–6.4 quality control; iv) 6.5–8.0 process control; v) $>$ 8.1 any application (Williams & Norris, 2001). Considering the RPD values achieved in this study, the PLS models could be suitable for screening of quality.

Overall, the prediction results are in agreement with or better than those reported in literature (Afonso et al., 2022; Feng et al., 2011; McGlone et al., 2007) for yellow kiwi in the Vis/NIR spectral range (SSC: R_P^2 from 0.81 to 0.92; FH: R_P^2 from 0.84 to 0.88; FF: $R_P^2 = 0.57$; DM: R_P^2 from 0.65 to 0.91). Especially for FF, the approach proposed in the present study showed notable improvements (R_P^2 until 0.866). Compared to SSC and DM, FF is associated with minor changes in chemical composition, such as pectin levels. Consequently, it is unlikely that NIR can be directly applied to detect these minor chemical changes in fruit. Furthermore, modifications in firmness could be also associated with change in cell wall adherence, and thus in cell shape modifications. This could result in changes in light scattering within the fruit that are detectable as a change in apparent absorbance variations. However, there is not a consistent link between scattering and firmness. Considering of all this and that FF is correlated to a range of other attributes, from pigment level to water content and starch-sugar conversion, secondary correlations in the Vis/NIR ranges are likely to be the most useful (Subedi & Walsh, 2009).

Considering literature data, Ciccoritti et al. (2019), using a spectrometer working from 850 to 2500 nm, reported the best results for SCC and DM prediction. However, a comparison with our results may not be appropriate for several reasons. First of all, Ciccoritti et al. (2019) studied green-fleshed kiwifruit varieties and not yellow flesh kiwifruit, and the quality parameters were evaluated during storage (until 90 days) and not at harvest. The SSC and DM ranges were quite different, and, in our opinion, not comparable.

From an industrial point of view, in the light of the results obtained herein, the combination of Vis/NIR hyperspectral and NIR spectrometric techniques may be considered for possible application on real-time yellow kiwi selection lines. The two spectral ranges (400–1000 and 900–2500 nm), characterised by different penetration depth and overlapping signals, would allow to contemporary evaluate internal, dimensional, and surface parameters (e.g. colour or any defects identifiable with RGB images). This present study focused on internal quality parameters, and image processing is a well known technique to evaluate

and classify fruit according to external quality (Rocha, Hauagge, Wainer, & Goldenstein, 2009; Davies, 2009). Furthermore, Vis/NIR (408-117 nm) hyperspectral imaging was used to detect hidden bruises on kiwi fruit, which is a foundation for further development of an in-line inspection system (Ebrahimi et al., 2023; Lu & Tang, 2012).

5. Conclusions

In this study, the use of data fusion of Vis/NIR hyperspectral imaging and FT-NIR spectroscopy to non-destructively predict the quality parameters of yellow flesh "Jintao" kiwifruit was investigated. Data fusion improved the prediction power of PLS models, with a mean RMSEP reduction of 16.0 ± 4.8%. The best results were achieved using a mid-level data fusion approach, which combines the scores from PCA or PLS models developed for each data set. The results of this study suggest that data fusion is a promising approach to improve the non-destructive prediction of quality parameters in yellow flesh kiwifruit. This could be useful for growers and retailers to optimise the harvesting time and ensure that fruits are harvested at the optimal stage of maturity. Further studies are needed to investigate the use of data fusion to predict other relevant quality parameters on other vegetables, which have not been considered in the scientific literature.

Author contributions

Chiara Cevoli: Conceptualisation, Methodology, Investigation, Data curation, Formal analysis, Validation, Writing–original draft, Writing–review & editing. **Eleonora Iaccheri**: Conceptualisation, Methodology, Investigation, Data curation, Writing–original draft. **Angelo Fabbri**: Writing–review & editing. Methodology. **Luigi Ragni**: Conceptualisation, Writing– review & editing.

Declaration of competing interest

The authors declare that they have no known competing financial interests or personal relationships that could have appeared to influence the work reported in this paper.

Appendix A. Supplementary data

Supplementary data to this article can be found online at https://doi.org/10.1016/j.biosystemseng.2023.12.011.

References

Afonso, A. M., Antunes, M. D., Cruz, S., Cavaco, A. M., & Guerra, R. (2022). Non-destructive follow-up of 'Jintao' kiwifruit ripening through VIS-NIR spectroscopy – individual vs. average calibration model's predictions. *Postharvest Biology and Technology, 188*, Article 111895. https://doi.org/10.1016/j.postharvbio.2022.111895

ASABE Standard. (2018). *ASAE S368.4 DEC2000 (R2018) - compression test of food materials of convex shape*. American Society of Agricultural and Biological Engineers 2000.

Benelli, A., Cevoli, C., Fabbri, A., & Ragni, L. (2022). Ripeness evaluation of kiwifruit by hyperspectral imaging. *Biosystems Engineering, 223*, 42–52. https://doi.org/10.1016/j.biosystemseng.2021.08.009

Berardinelli, A., Iaccheri, E., Franceschelli, L., Tartagni, M., & Ragni, L. (2021). Non-destructive assessment of kiwifruit flesh firmness by a contactless waveguide device and multivariate regression analyses. *IEEE Journal on Emerging and Selected Topics in Circuits and Systems, 11*, 515–522. https://doi.org/10.1109/JETCAS.2021.3097095

Biancolillo, A., Boqué, R., Cocchi, M., & Marini, F. (2019). Data fusion strategies in food analysis. In M. Cocchi (Ed.), *Data fusion methodology and applications* (pp. 274–310). Amsterdam, Netherlands: Elsevier.

Brown, S. D. (2020). Data and model fusion chemometrics. In S. Brown, R. Tauler, & B. Walczak (Eds.), *Comprehensive chemometrics* (2nd ed., Vol. 3, pp. 317–335). Amsterdam, Netherlands: Elsevier.

Ciccoritti, R., Paliotta, M., Amoriello, T., & Carbone, K. (2019). FT-NIR spectroscopy and multivariate classification strategies for the postharvest quality of green-fleshed kiwifruit varieties. *Scientia Horticulturae, 257*, Article 108622. https://doi.org/10.1016/j.scienta.2019.108622

Daszykowski, M., Walczak, B., & Massart, D. L. (2002). Representative subset selection. *Analytica Chimica Acta, 468*, 91–103. https://doi.org/10.1016/S0003-2670(02)00651-7

Davies, E. R. (2009). The application of machine vision to food and agriculture: A review. *The Imaging Science Journal, 57*. https://doi.org/10.1179/174313109X454756, 197–21.

Ebrahimi, S., Pourdarbani, R., Sabzi, S., Rohban, M. H., & Arribas, J. I. (2023). From harvest to market: Non-destructive bruise detection in kiwifruit using convolutional neural networks and hyperspectral imaging. *Horticulturae, 9*, 936. https://doi.org/10.3390/horticulturae9080936

ElMasry, G., Wang, N., ElSayed, A., & Ngadi, M. (2007). Hyperspectral imaging for nondestructive determination of some quality attributes for strawberry. *Journal of Food Engineering, 81*, 98–107. https://doi.org/10.1016/j.jfoodeng.2006.10.016

Feng, J., Mcglone, A. V., Currie, M., Clark, C. J., & Jordan, B. R. (2011). Assessment of yellow-fleshed kiwifruit (*Actinidia chinensis* 'Hort16A') quality in pre-and post-harvest conditions using a portable near-infrared spectrometer. *HortScience, 46*, 57–63. https://doi.org/10.21273/HORTSCI.46.1.57

Lammertyn, J., Peirs, A., De Baerdemaeker, J., & Nicolaï, B. (2000). Light penetration properties of NIR radiation in fruit with respect to non-destructive quality assessment. *Postharvest Biology and Technology, 18*, 121–132. https://doi.org/10.1016/S0925-5214(99)00071-X

Li, X., Cai, M., Li, M., Wei, X., Liu, Z., Wang, J., Jia, K., & Han, Y. (2023). Combining Vis-NIR and NIR hyperspectral imaging techniques with a data fusion strategy for the rapid qualitative evaluation of multiple qualities in chicken. *Food Control, 145*, Article 109416. https://doi.org/10.1016/j.foodcont.2022.109416

Li, Q., Huang, Y., Zhang, J., & Min, S. (2021). A fast determination of insecticide deltamethrin by spectral data fusion of UV–vis and NIR based on extreme learning machine. *Spectrochimica Acta, Part A: Molecular and Biomolecular Spectroscopy, 247*, Article 119119. https://doi.org/10.1016/j.saa.2020.119119

Lu, Q., & Tang, M. (2012). Detection of hidden bruise on kiwi fruit using hyperspectral imaging and parallelepiped classification. *Procedia Environmental Sciences, 12*, 1172–1179. https://doi.org/10.1016/j.proenv.2012.01.404

McGlone, V. A., Clark, C. J., & Jordan, R. B. (2007). Comparing density and VNIR methods for predicting quality parameters of yellow-fleshed kiwifruit (*Actinidia chinensis*). *Postharvest Biology and Technology, 46*, 1–9. https://doi.org/10.1016/j.postharvbio.2007.04.003

McGlone, V. A., & Kawano, S. (1998). Firmness, dry-matter and soluble-solids assessment of postharvest kiwifruit by NIR spectroscopy. *Postharvest Biology and Technology, 13*, 131–141. https://doi.org/10.1016/S0925-5214(98)00007-6

Mishra, P., Marini, F., Brouwer, B., Roger, J. M., Biancolillo, A., Woltering, E., & van Echtelt, E. H. (2021). Sequential fusion of information from two portable spectrometers for improved prediction of moisture and soluble solids content in pear fruit. *Talanta, 223*, Article 121733. https://doi.org/10.1016/j.talanta.2020.121733

O'Toole, M. D., Marsh, L. A., Davidson, J. L., Tan, Y. M., Armitage, D. W., & Peyton, A. J. (2015). Non-contact multi-frequency magnetic induction spectroscopy system for industrial-scale bio-impedance measurement. *Measurement Science and Technology, 26*, Article 035102. https://doi.org/10.1088/0957-0233/26/3/035102

Qiang, L., Mingjie, T., Jianrong, C., Huazhu, L., & Chaitep, S. (2010). Selection of efficient wavelengths in NIR spectrum for determination of dry matter in kiwi fruit. *Maejo International Journal of Science and Technology, 4*, 113–124.

Ragni, L., Berardinelli, A., & Guarnieri, A. (2010). Impact device for measuring the flesh firmness of kiwifruits. *Journal of Food Engineering, 96*, 591–597. https://doi.org/10.1016/j.jfoodeng.2009.09.006

Ragni, L., Cevoli, C., Berardinelli, A., & Silaghi, F. A. (2012). Non-destructive internal quality assessment of "hayward" kiwifruit by waveguide spectroscopy. *Journal of Food Engineering, 109*, 32–37. https://doi.org/10.1016/j.jfoodeng.2011.10.002

Rocha, A., Hauagge, D. C., Wainer, J., & Goldenstein, S. (2009). Automatic fruit and vegetable classification from images. *Computers and Electronics in Agriculture, 70*, 96–104. https://doi.org/10.1016/j.compag.2009.09.002

Schaare, P. N., & Fraser, D. G. (2000). Comparison of reflectance, interactance and transmission modes of visible-near infrared spectroscopy for measuring internal properties of kiwifruit (Actinidia chinensis). *Postharvest Biology and Technology, 20*, 175–184. https://doi.org/10.1016/S0925-5214(00)00130-7

Serranti, S., Bonifazi, G., & Luciani, V. (2017). Non-destructive quality control of kiwi fruits by hyperspectral imaging. In *Proc. SPIE 10217, sensing for agriculture and food quality and safety IX*. https://doi.org/10.1117/12.2255055, 102170O (1 May 2017).

Shafie, K. A., Künnemeyer, R., McGlone, A., Talele, S., & Vetrova, V. (2015). An optimised six-wavelength model for predicting kiwifruit dry matter. *Journal of Near Infrared Spectroscopy, 23*, 103–109. https://doi.org/10.1255/jnirs.1151

Subedi, P. P., & Walsh, K. B. (2009). Non-invasive techniques for measurement of fresh fruit firmness. *Postharvest Biology and Technology, 51*, 297–304. https://doi.org/10.1016/j.postharvbio.2008.03.004

Testolin, R., & Ferguson, A. R. (2009). Kiwifruit (Actinidia spp.) production and marketing in Italy. *New Zealand Journal of Crop and Horticultural Science, 37*, 1–32. https://doi.org/10.1080/01140670909510246

Valero, C., Ruiz-Altisent, M., Cubeddu, R., Pifferi, A., Taroni, P., Torricelli, A., Valentini, G., Johnson, D. S., & Dover, C. J. (2004). Detection of internal quality in kiwi with time-domain diffuse reflectance spectroscopy. *Applied Engineering in Agriculture, 20*, 223–230. https://doi.org/10.13031/2013.15879

Williams, P. C., & Norris, K. (2001). *Near-infrared technology in the agricultural and food industries* (2nd ed.). St. Paul, MN: American Association of Cereal Chemists.

Yang, B., Guo, W., Li, W., Li, Q., Liu, D., & Zhu, X. (2019). Portable, visual, and nondestructive detector integrating Vis/NIR spectrometer for sugar content of kiwifruits. *Journal of Food Process Engineering, 42*, Article e12982. https://doi.org/10.1111/JFPE.12982

Zhu, H., Chu, B., Fan, Y., Tao, X., Yin, W., & He, Y. (2017). Hyperspectral imaging for predicting the internal quality of kiwifruits based on variable selection algorithms and chemometric models. *Scientific Reports: Nature, 7*, 7845. https://doi.org/10.1038/s41598-017-08509-6